Chapter 2

Crystallographic Analysis of Complex Materials

Chapter Outline

2.1. THEORETICAL BACKGROUND

2.1.1. Scattering Intensity

In powder diffraction experiments, one directs a beam or ray of particles at the sample (Fig. 2.1) and measures the intensity of the scattered beam as a function of scattering angle, 2θ, and the wavelength of the probe. The procedures to carry out such measurements are discussed in Chapter 4. The task of the

Pergamon Materials Series, Vol. 16. http://dx.doi.org/10.1016/B978-0-08-097133-9.00002-2

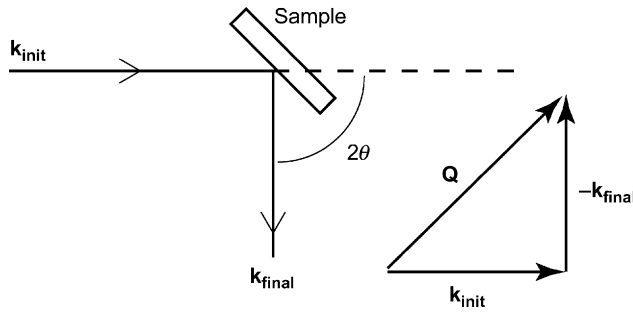

FIGURE 2.1 Geometry of the powder diffraction measurement and definition of the scattering vector, **Q**.

researcher is to analyze the intensity data and relate them to the structure or dynamics of the sample. The analysis is usually made in two stages. The first stage is to correct the observed intensity for secondary effects such as absorption and background, etc., to obtain a normalized intensity that can be theoretically analyzed. The second is to explain and numerically reproduce the normalized intensity using a structural model. These steps are discussed in Chapters 5 and 6. Before these subjects are introduced, we will first present the theoretical basis in this chapter and introduce the PDF method in Chapter 3. From this chapter to Chapter 7, pages are crowded with equations that are sometimes long, but the meaning of each equation is relatively simple. They are all included in the software used in the analysis that can be downloaded to your computer.

X-rays and neutrons interact relatively weakly with atoms, which makes the measurement hard, since the scattered intensity is weak, but at the same time makes the data analysis easy. This should be contrasted to the case of electrons that interact with atoms more strongly, which makes the signal stronger but the analysis harder. Traditionally, powder diffraction and PDF analysis have predominantly been carried out using X-rays and neutrons, but recent developments, building on earlier work principally on amorphous films (Moss and Graczyk, 1969; Cockayne, 2007), indicate that PDFs derived from electrons are of sufficient quality to yield quantitative local structural information from nanomaterials (Abeykoon *et al.*, 2012). This has the potential for greatly expanding the use of PDF analysis as a basic characterization tool used in chemistry and materials science laboratories synthesizing nanomaterials. Transmission electron microscopy (TEM), both low and high resolution, has for a long time been a standard tool for "seeing" what was obtained in a nanoparticle synthesis. Now, electron diffraction data from the same sample collected on a standard laboratory TEM can be processed to obtain PDFs (Abeykoon *et al.*, 2012) that give highly complementary information to the images by giving quantitative bond-lengths and structural information averaged over the whole sample in the beam. More reliably accurate PDFs will

still be obtained from X-ray or neutron data obtained from powerful synchrotron X-ray and neutron sources, but the ability to rapidly collect PDF quality data from an in-laboratory electron source qualitatively changes how researchers can use the method. As well as the carefully planned and executed detailed materials studies carried out these days, rapid measurements can also be made to assess sample quality of a particular batch or to make a rapid comparison of samples made using different approaches, for example. The theory behind X-ray, neutron, and electron PDFs is largely the same, based on the weak-scattering kinematical scattering equations, and is developed in a general sense in this and in the next chapter. Different aspects of data collection and analysis for X-rays, neutrons, and electrons are discussed in Chapters 4 and 5.

The total intensity of the scattered X-ray, neutron, or electron beam, I_T, is composed of several parts:

$$I_T = I_C + I_{IC} + I_{MC} + I_{BG} \tag{2.1}$$

where I_C is the coherent scattering intensity, I_{IC} the incoherent scattering intensity, I_{MC} the multiple-scattering intensity, and I_{BG} the background intensity. The scattering intensity I_T is measured as a function of the scattering angle, 2θ, and the wavelength of the probe, λ. For elastic scattering, the diffraction vector, $\mathbf{Q}$, defined in Section 1.1.5 and Fig. 2.1, has a magnitude

$$|\mathbf{Q}| = \frac{4\pi \sin\theta}{\lambda} \tag{2.2}$$

where λ is the wavelength of the scattered particle and $\theta = 2\theta/2$, where 2θ is the angle between the incident and diffracted beams. In the case of powder measurements, the only relevant quantity is the magnitude of the diffraction vector, $Q = |\mathbf{Q}|$. We note that since $\sin\theta \leq 1$, the experimentally accessible range for Q is limited to less than $4\pi/\lambda$. For instance, Cu K_α radiation, which is most widely used in laboratory X-ray facilities, has a wavelength of 1.54 Å. This means the range of Q is limited to about 8 $Å^{-1}$, while for most of the applications discussed in this book, the Q range of $\sim$20–40 $Å^{-1}$ is preferred. This is an important point that will be discussed in Chapter 3.

Incoherent scattering arises from Compton scattering in the case of X-rays and nuclear spin scattering in the case of neutrons. Multiple scattering occurs mainly within the sample, but double scattering involving the sample and the environment can be significant. The background intensity here includes scattering without the sample, due to the sample holder, air, optical systems, etc. This is different from the so-called "background" in crystallographic analysis, the intensity in between the Bragg peaks, which also includes diffuse scattering from the sample. In most crystallographic analyses, the "background" is curve-fitted and discarded. But, as we will see, the diffuse scattering intensity contains a wealth of information about local structure, and in this context, discarding the diffuse scattering amounts to throwing the baby out with the bathwater. The subtitle of this book, Underneath the Bragg Peaks, implies

the importance of the diffuse scattering intensity, which is usually overlooked in standard crystallographic analysis. Note that in the PDF method, the true background intensity has to be independently measured by carrying out a scattering measurement without a sample.

The information on structure and lattice dynamics is contained in the coherent scattering, I_C, which can be expressed in the form of a scattering cross-section, $d\sigma_C/d\Omega$. Here, $d\Omega$ is the solid angle that the detector subtends with the origin where the sample is located. The formalism of "scattering cross-sections" is introduced and defined more formally in Appendices 2.1 and 5.1.[1] The experimentally measured intensity of coherent scatting, I_C, is related to $d\sigma_C/d\Omega$, but is modified by absorption and polarization factors;

$$I_C = APC\frac{d\sigma_C}{d\Omega}. \tag{2.3}$$

The absorption factor, A, depends on the geometry of the sample and the nature of the scattering particle. More detailed discussions on this factor are given in Chapter 5. The electric polarization factor for X-rays and spin polarization factor for neutrons are well known and will not be repeated here (e.g., see Warren, 1990; Bacon, 1975, respectively). C is the normalization factor needed to express $d\sigma_C/d\Omega$ in the appropriate units of intensity per atom. In the following, we focus on $d\sigma_C/d\Omega$ and discuss how to obtain the structural information from this quantity.

2.1.2. Sample Scattering Amplitude

For most of this book, we need a surprisingly small amount of basic theoretical background. The only equation that truly needs to be understood is that for the sample scattering amplitude,

$$\Psi(\mathbf{Q}) = \frac{1}{\langle b\rangle}\sum_v b_v e^{i\mathbf{Q}\cdot\mathbf{R}_v}, \tag{2.4}$$

where $\mathbf{Q}$ is the diffraction vector or the momentum transfer, and is defined by[2]

1. The concept of the scattering cross-section is a very useful one which relates a sample-dependent property (the probability of a particular scattering event occurring) to a real experimental value (the number of detected counts in a detector). For those readers unfamiliar with it, we recommend spending a short time to understand and get comfortable with the basic ideas (see Section A5.1.1 in Appendix 5.1 as well as standard textbooks). Do not be put off by the mathematical looking nature of the expressions, an unfortunate legacy of its origin in theoretical physics. The ideas behind the scattering cross-section are highly intuitive and physical.

2. Note that in some textbooks, $\mathbf{Q}$ is defined as $\mathbf{Q} = k_{final} - k_{init}$, that is, with the opposite sign as used here. This is fine, though in that case, Eq. (2.4) becomes $\Psi(\mathbf{Q}) = \frac{1}{\langle b\rangle}\sum_v b_v e^{-i\mathbf{Q}\cdot\mathbf{R}_v}$ and Eq. (2.12) becomes $\mathbf{Q} = -\mathbf{K}$.

$$\mathbf{Q} = \mathbf{k}_{\text{init}} - \mathbf{k}_{\text{final}} \tag{2.5}$$

where $\mathbf{k}_{\text{init}}$ ($|\mathbf{k}_{\text{init}}| = 2\pi/\lambda_{\text{init}}$) is the wavevector of the incoming beam, and $\mathbf{k}_{\text{final}}$ ($|\mathbf{k}_{\text{final}}| = 2\pi/\lambda_{\text{final}}$) is the wavevector of the scattered beam (Fig. 2.1). For elastic scattering $\lambda_{\text{init}} = \lambda_{\text{final}}$, thus, the magnitude of $\mathbf{Q}$ is given,

$$Q = |\mathbf{Q}| = 2k\sin\theta = \frac{4\pi\sin\theta}{\lambda} \tag{2.6}$$

where $k = |\mathbf{k}_{\text{init}}| = |\mathbf{k}_{\text{final}}|$.

For X-rays and electrons, b_v depends fairly strongly on Q and is usually denoted as $f(Q)$, but for neutrons b_v is independent of Q. This difference reflects the quite different spatial spread of the scatterer, electron density for X-rays, electric potential for electrons, and nucleus for neutrons. The angle brackets around the b in the denominator indicate an average over all the atoms in the sample. This is defined more precisely in Chapter 3.

In solids, atoms are not static, but are vibrating due to atomic vibration. Consequently, $\mathbf{R}_v$ changes with time, and $\Psi(\mathbf{Q})$ really is a function of time,

$$\Psi(\mathbf{Q},t) = \frac{1}{\langle b\rangle}\sum_v b_v e^{i\mathbf{Q}\cdot\mathbf{R}_v(t)}. \tag{2.7}$$

However, in the following, we suppress the variable t, unless noted, for the sake of simplicity. The time-dependent structure factor will be discussed in the next section when we introduce the Debye–Waller (DW) approximation and in Chapter 7 in relation to inelastic scattering.

The derivation of Eq. (2.4) is given in Appendix 2.2 in two different ways, one intuitive and the other more formal. In deriving this result, only single scattering of the incident beam with the atoms was considered and coherent multiple scattering was neglected. This simplification is known as the kinematic approximation and is accurate only when the scattering is weak and the structural coherence is not too large as in powders. In highly perfect large crystals, coherent multiple scattering often is as important as single scattering, and they together can create dramatic effects such as anomalous transmission. In such a case, the diffraction phenomena can be described accurately only by the dynamical scattering theory. This is the situation that normally prevails in electron diffraction and, since the PDF equations are based on the kinematical scattering equations, is the main reason why there has hitherto not been a focus on obtaining PDFs from electron diffraction data. In this book, we do not enter this subject, since we are concerned with imperfect crystals that do not require dynamical theories.

In general, the Fourier transform of a function $f(\mathbf{x})$ is given by $F(\mathbf{Q}) = \sum_{j-\infty}^{\infty} f(\mathbf{x}_j)e^{i\mathbf{k}\cdot\mathbf{x}_j}$. Upon inspection of Eq. (2.4), it is evident that $\Psi(\mathbf{Q})$ is just the Fourier transform of the atomic position, $\mathbf{R}_v$. The structural information is contained in the phase of the exponential factor. Thus, if we

know this scattering amplitude, we can determine the atomic structure exactly, merely by taking the inverse Fourier transformation of $\Psi(\mathbf{Q})$. Crystallography would be a trivial task if that was possible. However, as is well known, we cannot directly measure the scattered amplitude $\Psi(\mathbf{Q})$ but only the intensity of the diffracted beam, which is directly related to the square of the magnitude of $\Psi(\mathbf{Q})$, that is, $|\Psi(\mathbf{Q})|^2$. In detail,

$$\frac{\mathrm{d}\sigma_{\mathrm{C}}(\mathbf{Q})}{\mathrm{d}\Omega} = \frac{\langle b\rangle^2}{N}|\Psi(\mathbf{Q})|^2 = \frac{1}{N}\sum_{\nu,\mu} b_\nu b_\mu \mathrm{e}^{\mathrm{i}\mathbf{Q}\cdot\left(\mathbf{R}_\nu - \mathbf{R}_\mu\right)}. \tag{2.8}$$

As we discuss in greater detail in the next chapter, the total scattering structure function, $S(\mathbf{Q})$, which is Fourier transformed to obtain the PDF, is a normalized form of this cross-section, specifically

$$\langle b\rangle^2 S(\mathbf{Q}) = \frac{\mathrm{d}\sigma_C}{\mathrm{d}\Omega} + \langle b\rangle^2 - \langle b^2\rangle. \tag{2.9}$$

As the measured intensity is proportional to the square of the scattering amplitude, $\Psi(\mathbf{Q})$, the phase information of $\Psi(\mathbf{Q})$ is lost. All that survives is the phase difference between scattering events from different atoms. Specialized indirect methods of recovering the lost phase information exist that make use of dynamical diffraction from perfect single crystals, substitution of heavy atoms at known locations in molecules, and using anomalous diffraction, for example. These are extraordinarily powerful techniques that have revolutionized the structure determination of solids and crystalline small and large molecular structures. The methods are mature for crystalline materials and are well described in other books, for example, Giacovazzo *et al*. (1992) or Woolfson (1997). The phase retrieval methods have been extended to the case of nonperiodic structures using a method called "oversampling" (Sayre, 1952) and demonstrated experimentally as a method called diffraction imaging (Miao *et al*., 1999; Zuo *et al*., 2003). It is difficult to get sufficient signal from small nanoparticles to get atomic resolution using this approach, along with difficulties in making the reconstruction. However, great progress is being made experimentally (with the advent of hard X-ray free electron lasers, STEM microscopes, and 180° tilting sample stages) and algorithmically so that this approach is set to have a much larger scientific impact in the coming years. Nonetheless, there are many real-world situations where this approach is not possible or does not give the required information, and it is necessary to have methods that can reconstruct 3D structural information from powder data in the absence of this phase information, the topic of this book. In this case, the structure must be reconstructed by creating a model structure and comparing the calculated scattering intensity from this structure with the measured structure function. Structure determination is not a trivial task, and invariably involves extensive data analysis and modeling.

For a perfectly periodic lattice (a crystal), the scattering amplitude becomes extremely simple because of the lattice sum formula. For a monotonic crystal in one-dimension, $R_v = va$, where a is the lattice repeat distance, and we get

$$\lim_{N\to\infty}\left(\frac{1}{N}\sum_{v=1}^{N} e^{iQva}\right) = \delta(Q - na^*), \tag{2.10}$$

where $\delta(z)$ denotes the Dirac delta-function, n is an integer and $a^* = 2\pi/a$. Derivation of this equation is also given in the standard textbooks. Thus in three dimensions, the scattering occurs only at a discrete set of wavevectors, $\mathbf{K}$, forming the reciprocal lattice,

$$\mathbf{K} = h\mathbf{a}^* + k\mathbf{b}^* + l\mathbf{c}^*, \tag{2.11}$$

where $\mathbf{a}^*$, $\mathbf{b}^*$, $\mathbf{c}^*$ are the reciprocal lattice vectors. The Bragg condition for allowed scattering now restricts $\mathbf{Q}$ to being equal to $\mathbf{K}$:

$$\mathbf{Q} = \mathbf{K}. \tag{2.12}$$

For more than one atom in the unit cell, we can denote

$$\langle \mathbf{R}_v \rangle - \langle \mathbf{R}_\mu \rangle = \mathbf{R}_k + \mathbf{r}_n - \mathbf{r}_m, \tag{2.13}$$

where $\mathbf{R}_k$ specifies the separation between the unit cells, and $\mathbf{r}_n$ and $\mathbf{r}_m$ are the position vectors of the nth and mth atoms within the unit cell. Then, from Eqs. (2.8) and (2.13), we get

$$\begin{aligned}\frac{d\sigma_C(\mathbf{Q})}{d\Omega} &= \frac{\delta(\mathbf{Q}-\mathbf{K})}{n_c}\sum_{n,m} b_n b_m e^{i\mathbf{Q}\cdot(\mathbf{r}_n-\mathbf{r}_m)} = \frac{\delta(\mathbf{Q}-\mathbf{K})}{n_c}\sum_{n,m} b_n b_m e^{i\mathbf{K}_{hkl}\cdot(\mathbf{r}_n-\mathbf{r}_m)} \\ &= \frac{\delta(\mathbf{Q}-\mathbf{K})}{n_c}\left|\sum_n b_n e^{i\mathbf{K}_{hkl}\cdot(\mathbf{r}_n)}\right|^2,\end{aligned} \tag{2.14}$$

where the sum over n is now taken only over all the atoms in the unit cell, n_c. The term

$$F_{hkl} = \sum_n b_n e^{i\mathbf{K}_{hkl}\cdot(\mathbf{r}_n)} \tag{2.15}$$

is the well-known crystallographic structure factor that gives the intensity of the Bragg peak located at $\mathbf{Q} = \mathbf{K}_{hkl}$, where h, k, and l are the integers defining the particular reciprocal lattice vector in Eq. (2.11). Thus by determining $\mathbf{K}$, or the position of the Bragg peak in the reciprocal space, the lattice constants and symmetry are directly known. The intensity of the Bragg peak, Eq. (2.14), translates to the atomic positions within the unit cell. An example of the structure function $S(Q)$ for a crystalline powder

sample ($LaMnO_3$) is shown in Fig. 3.1a.The enormous simplification in the problem that comes about when the sample is crystalline is evident by comparing Eqs. (2.8) and (2.14). In the former, general case, the sums run over all the atoms in the sample; in the latter, crystalline case, the double sum runs only over the atoms in the unit cell. It is this more complicated situation, when the structure is not perfectly periodic and Eq. (2.14) no longer strictly applies, that is the main subject of this book. Furthermore, in the actual measurement, the intensity is modified by absorption, polarization, and other factors. The total intensity of the scattered beam includes contributions from the multiple scattering, inelastic scattering, and background due to sample holders and containers. These effects will be discussed in stages throughout this book.

2.1.3. DW Approximation

As has been repeated numerous times, the assumption of perfect periodicity is the centerpiece for crystallography. However, a crystal structure is never perfectly periodic even when the crystal is perfect because atoms are vibrating due to either thermal or zero-point quantum vibrations. The DW approximation was developed to incorporate the effect of lattice vibrations and is an integral part of the crystallographic analysis.

We will start with the time-dependent scattering amplitude, Eq. (2.8). As the position of the atom, $\mathbf{R}$, changes with time, it is convenient to describe it in terms of the deviation from the average position, $\mathbf{R}(t) = \mathrm{u}(t) + \langle\!\langle R \rangle\!\rangle$, where $\mathbf{u}$ is the deviation and $\langle\!\langle \mathbf{R} \rangle\!\rangle$ is the time-averaged position of the atom. The subscript v is suppressed for simplicity. Eq. (2.8) will now be, after averaging over time (denoted by $\langle\!\langle \cdots \rangle\!\rangle$),

$$\begin{aligned}\langle\!\langle e^{i\mathbf{Q}\cdot\mathbf{R}} \rangle\!\rangle &= \langle\!\langle e^{i\mathbf{Q}\cdot(\langle\!\langle \mathbf{R} \rangle\!\rangle + \mathbf{u})} \rangle\!\rangle = e^{i\mathbf{Q}\cdot\langle\!\langle \mathbf{R} \rangle\!\rangle} \langle\!\langle e^{i\mathbf{Q}\cdot\mathbf{u}} \rangle\!\rangle, \\ &= e^{i\mathbf{Q}\cdot\langle\!\langle \mathbf{R} \rangle\!\rangle} \left[1 + i\langle\!\langle \mathbf{Q}\cdot\mathbf{u} \rangle\!\rangle - \frac{1}{2}\langle\!\langle (\mathbf{Q}\cdot\mathbf{u})^2 \rangle\!\rangle + \cdots \right]. \end{aligned} \tag{2.16}$$

As $\langle\!\langle \mathbf{Q}\cdot\mathbf{u} \rangle\!\rangle = \mathbf{Q}\cdot\langle\!\langle \mathbf{u} \rangle\!\rangle = 0$ by definition, if $\mathbf{u}$ is small enough, this approximates rather nicely to the expression for a Gaussian function, and we get,

$$\langle\!\langle e^{i\mathbf{Q}\cdot\mathbf{R}} \rangle\!\rangle \approx e^{i\mathbf{Q}\cdot\langle\!\langle \mathbf{R} \rangle\!\rangle} e^{-W} = e^{i\mathbf{Q}\cdot\langle\!\langle \mathbf{R} \rangle\!\rangle} e^{-\frac{1}{2}Q^2\langle\!\langle u^2 \rangle\!\rangle}, \tag{2.17}$$

where e^{-W} is called the DW factor. It can also be shown (Warren, 1990) that if the probability distribution of $\mathbf{u}$ is Gaussian then this DW approximation is also exact even if $\mathbf{u}$ is not small. It is clear from this that the effect of lattice vibrations is not to broaden out the Bragg peaks. The Bragg peaks remain perfectly sharp but their intensity is diminished by the factor $\exp\left(-\frac{1}{2}Q^2\langle u^2 \rangle\right)$. Thus, if the vibrational amplitude of each atom is equal, the structure function becomes

$$S(\mathbf{Q}) = \mathrm{e}^{-\langle\langle u^2\rangle\rangle Q^2} S_0(\mathbf{Q}) + 1 - e^{-\langle\langle u^2\rangle\rangle Q^2},$$

$$S_0(\mathbf{Q}) = \frac{\delta(\mathbf{Q}-\mathbf{K})}{\langle b\rangle^2}\left[\sum_{\nu,\mu} b_\nu b_\mu \mathrm{e}^{\mathrm{i}\mathbf{Q}\cdot\left(\langle\langle\mathbf{R}_\nu\rangle\rangle - \langle\langle\mathbf{R}_\mu\rangle\rangle\right)} - \langle b^2\rangle + \langle b\rangle^2\right]. \tag{2.18}$$

We will discuss in Chapter 7 why the term $[1-\exp(-\langle\langle u^2\rangle\rangle Q^2)]$ was added in Eq. (2.18) (see Eq. 7.24). This term approximately describes the diffuse inelastic scattering intensity due to phonons.

It should be noted that the assumption in the approximation in Eq. (2.17) is that the distribution of u is described as a Gaussian distribution. Whenever this assumption is violated, the DW approximation cannot be accurate. The structure function of the average lattice sites, $S_0(Q)$, is composed of delta functions that spread over the entire Q-space. However, because of the DW factor, the intensity decreases with increasing $\mathbf{Q}$, and the Bragg peaks practically disappear beyond certain values of $\mathbf{Q}$.

2.1.4. Diffuse Scattering

The DW factor reduces the intensities of the Bragg scattering (Eq. 2.18) but where does the lost intensity go? It appears in between the Bragg peaks and becomes what is called diffuse scattering. The diffuse intensity is often hard to see and measure. It is widely spread over Q-space, compared to the Bragg peaks that are strongly confined at reciprocal lattice points in Q-space. However, a significant proportion of the total integrated intensity can reside in the diffuse scattering. Indeed, in the high-Q region where the Bragg peaks are small due to the DW factor, the scattering is predominantly diffuse.

In powder measurements, the diffuse scattering is slowly varying with $\mathbf{Q}$ and forms a continuous background which is usually discarded in crystallographic analyses. However, the diffuse scattering provides important information regarding the local deviations from the average structure. The subtitle of this book, Underneath the Bragg Peaks, is meant to emphasize the importance of this diffuse scattering intensity which is usually not given the attention it deserves.

In this section, we will explain how the diffuse scattering arises and what information it carries. This is a conventional treatment and a full understanding of it is not needed to understand the PDF. It is included for those readers who are comfortable with scattering equations and want an intuitive idea of how defects in crystals affect the measured scattering. One of the beneficial features of PDF analysis is that the structural information in the diffuse scattering appears in a direct and intuitive way, circumventing the need to grapple with the mathematics of diffuse scattering presented here. First time readers can skip directly to Section 2.2 without loss of continuity. Ultimately, it is

very helpful to develop an understanding of the relationship between defects and diffuse scattering, from the equations presented here. It is also possible to develop an intuitive understanding of this relationship using the online diffraction tutorials at www.lks.physik.uni-erlangen.de/diffraction/. These allow the user to calculate the diffuse scattering patterns interactively from different arrangements of atoms and defects within simulated crystals.

Here we consider the diffuse scattering in a crystalline material. The starting point is again the scattering amplitude, Eq. (2.4). We assume that the position of the vth atom, $\mathbf{R}_v$, deviates from the ideal crystallographic site, $\mathbf{R}_v^0$, by $\mathbf{u}_v$;

$$\mathbf{R}_v = \mathbf{R}_v^0 + \mathbf{u}_v. \tag{2.19}$$

Thus, the scattering amplitude is

$$\Psi(\mathbf{Q}) = \frac{1}{\langle b \rangle} \sum_v \mathrm{b}_v \mathrm{e}^{\mathrm{i}\mathbf{Q}\cdot\mathbf{R}_v} = \frac{1}{\langle b \rangle} \sum_v \mathrm{b}_v \mathrm{e}^{\mathrm{i}\mathbf{Q}\cdot\mathbf{R}_v^0} [1 + \mathrm{i}\mathbf{Q}\cdot\mathbf{u}_v + \cdots], \tag{2.20}$$

where we have made the same expansion as we did in Eq. (2.16). We can then consider the intensity contributions to $\Psi(\mathbf{Q})$ term by term:

$$\Psi(\mathbf{Q}) = \Psi_1(\mathbf{Q}) + \Psi_2(\mathbf{Q}) + \cdots, \tag{2.21}$$

where

$$\Psi_1(\mathbf{Q}) = \frac{1}{\langle b \rangle} \sum_v b_v \mathrm{e}^{\mathrm{i}\mathbf{Q}\cdot\mathbf{R}_v^0}, \quad \Psi_2(\mathbf{Q}) = \frac{1}{\langle b \rangle} \sum_v \mathrm{i}\mathbf{Q}\cdot\mathbf{u}_v b_v \mathrm{e}^{\mathrm{i}\mathbf{Q}\cdot\mathbf{R}_v^0}, \tag{2.22}$$

and so on. The first term describes the Bragg scattering. If we apply volume averaging to the second term in the bracket of Eq. (2.20), just as in Eq. (2.16), it disappears because, by definition, $\langle\langle u \rangle\rangle = 0$. However, this kind of mean-field approximation as we discussed in Chapter 1 is a case of throwing the baby out with the bathwater. Actually, if we examine Eq. (2.22), we see that $\Psi_2(\mathbf{Q})$ is not zero when these deviations are locally correlated. This can be understood by applying the Fourier expansion to $\mathbf{u}_v$,

$$\mathbf{u}_v\left(\mathbf{R}_v^0\right) = \frac{1}{\sqrt{N}} \sum_{\mathbf{q}} \mathbf{u}_q \mathrm{e}^{\mathrm{i}\mathbf{q}\cdot\mathbf{R}_v^0}. \tag{2.23}$$

Then the second term in Eq. (2.22) becomes

$$\Psi_2(\mathbf{Q}) = \frac{\mathrm{i}}{\langle b \rangle} \sum_v b_v \mathrm{e}^{\mathrm{i}\mathbf{Q}\cdot\mathbf{R}_v^0} \mathbf{Q}\cdot\mathbf{u}_v = \frac{\mathrm{i}}{\sqrt{N}\langle b \rangle} \sum_{v,q} b_v \mathbf{Q}\cdot\mathbf{u}_q \mathrm{e}^{\mathrm{i}(\mathbf{Q}-\mathbf{q})\cdot\mathbf{R}_v^0}. \tag{2.24}$$

Again the lattice sum (Eq. 2.10) results in

$$\Psi_2(\mathbf{Q}) = \frac{i\sqrt{N}}{\langle b \rangle} \sum_q g(\mathbf{K})\left(\mathbf{Q}\cdot\mathbf{u}_q\right)\delta(\mathbf{Q} - \mathbf{q} - \mathbf{K}), \tag{2.25}$$

where $g(\mathrm{K}) = (1/N)\sum_n b_n \mathrm{e}^{\mathrm{i}\mathbf{K}\cdot\mathbf{R}_n^0}$, with n running over atoms in the unit cell. As before, $\mathbf{K}$ is the reciprocal lattice vector, Eq. (2.11). The intensity will be

$$I(\mathbf{Q}) = I_{\mathrm{BG}}(\mathbf{Q}) + I_{\mathrm{D}}(\mathbf{Q}) + \cdots,$$
$$I_{\mathrm{D}}(\mathbf{Q}) = \frac{\langle b \rangle^2}{N} |\Psi_2(\mathbf{Q})|^2 = |g(\mathbf{K})|^2 |\mathbf{Q} \cdot \mathbf{u}_{\mathbf{Q}-\mathbf{K}}|^2, \tag{2.26}$$

where $I_{\mathrm{BG}}(\mathbf{Q})$ represents the Bragg diffraction intensity and $I_{\mathrm{D}}(\mathbf{Q})$ the diffuse scattering intensity. The cross-terms between Ψ_1 and Ψ_2 vanish because of the two different δ-functions involved. While the Bragg peak appears at the reciprocal lattice point where $\mathbf{Q} = \mathbf{K}$, diffuse scattering appears at $\mathbf{Q} = \mathbf{K} + \mathbf{q}$, at a point separated by $\mathbf{q}$ from the Bragg peak. If there is only one $\mathbf{q}$ value for which $\mathbf{u}_{\mathbf{q}}$ is nonzero, we have a modulated structure with the wave vector $\mathbf{q}$. If the deviations are local, a range of $\mathbf{q}$ vectors are needed to describe the structure. For instance, if the deviation occurs only at one atomic site, or delta-function in real space, then its Fourier transform covers the entire Q-space. That is why the scattering from a local object results in broadly spread diffuse scattering.

An example of diffuse scattering from a single crystal is shown in Fig. 2.2. The most common diffuse scattering is due to thermal vibration of atoms and is called thermal diffuse scattering (TDS). For a simple monatomic solid, the amplitude of thermal vibration is given in terms of the phonon density,

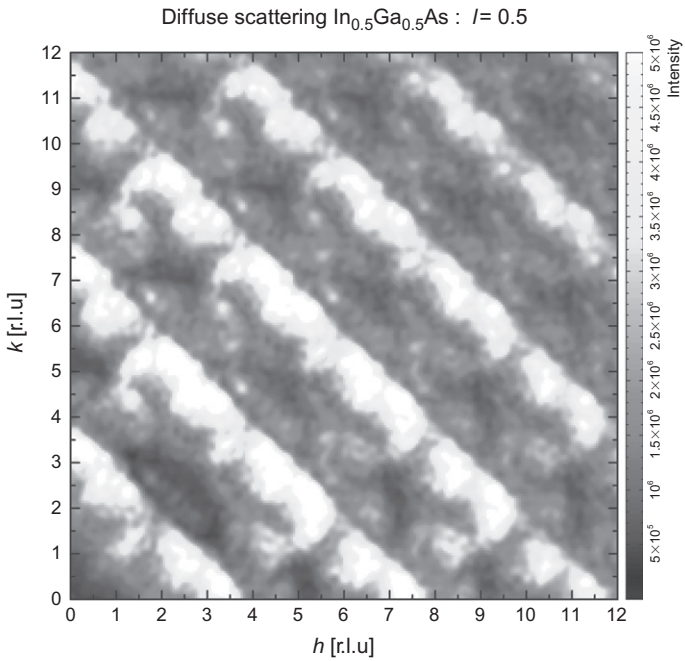

FIGURE 2.2 Example of diffuse scattering calculated for the (hk0.5) plane of reciprocal space is shown for the case of an $In_{0.5}Ga_{0.5}As$ alloy. Bright indicates strong intensity, dark weak intensity. Units are reciprocal lattice units (Jeong *et al.*, 2001).

$$\left\langle |\mathbf{Q}\cdot\mathbf{u}_\mathbf{q}|^2 \right\rangle = \frac{\hbar}{2M}\sum_j \frac{|\mathbf{Q}\cdot\boldsymbol{\varepsilon}_j(\mathbf{q})|^2}{\omega_j(\mathbf{q})}\left\{ n_j(\mathbf{q}) + \frac{1}{2}\right\}, \tag{2.27}$$

where M is the atomic mass, $j = 1,2,3$ indexes the three modes with polarization vector $\boldsymbol{\varepsilon}_j(\mathbf{q})$, $\omega_j(\mathbf{q})$ is the frequency of the phonon, and $n_j(q)$ is the phonon density,

$$n_j(\mathbf{q}) = \frac{1}{e^{\hbar\omega_j(\mathbf{q})/kT} - 1}. \tag{2.28}$$

This result is described in greater detail in the books on lattice vibrations (see Lattice Vibrations subheading at the end of this chapter). This result is reintroduced in Chapter 7 that deals with inelastic scattering. If the spectrometer has enough energy resolution to resolve phonon energy, the equations developed in Chapter 7 describe the inelastic scattering intensity. On the other hand, in the usual powder diffraction experiment, the diffractometer has no energy discrimination, so that Eqs. (2.27) and (2.28) are sufficient to describe the TDS.

Let us examine the case when q is sufficiently small and T is large so that $\hbar\omega_j(q) \ll kT$. In this limit, we are considering the long wavelength sound waves propagating in the solid:

$$\omega_j(\mathbf{q}) = c_j|\mathbf{q}|. \tag{2.29}$$

In this case,

$$\left\langle |\mathbf{Q}\cdot\mathbf{u}_\mathbf{q}|^2 \right\rangle \approx \frac{1}{2M}\sum_j \frac{|\mathbf{Q}\cdot\boldsymbol{\varepsilon}_j(\mathbf{q})|^2}{Q^2}\frac{Q^2}{q^2}\frac{kT}{c_j^2}. \tag{2.30}$$

Thus, the TDS intensity is proportional to T. From Eq. (2.27), it is clear that when $\mathbf{q}$ is parallel to $\mathbf{Q}$, only the longitudinal mode ($\boldsymbol{\varepsilon} \| \mathbf{q}$) is observed, while when $\mathbf{q}$ is perpendicular to $\mathbf{Q}$, only the transverse mode ($\boldsymbol{\varepsilon} \perp \mathbf{q}$) is observed. The TDS intensity in each case depends only on the sound velocity of each mode. As the TDS intensity is proportional to q^{-2} and diverges toward $q = 0$, it is strong only around the Bragg peak. The TDS pattern around each Bragg peak is similar, but its intensity increases with Q as Q^2. This is a common characteristic of displacive deviations. The local deviation may not take the form of local displacement, but atomic substitution, as in the case of alloying. In this case, the diffuse intensity does not increase with increasing Q and is similar for all the Bragg peaks, if it is corrected for the atomic scattering factor and the DW factor. For a multicomponent solid, the expression of the phonon intensity becomes more complex. This is discussed in Chapter 7.

Another important class of diffuse scattering is called Huang scattering (Huang, 1947; Borie, 1957, 1959, 1961) and originates from extended structural defects such as the strain fields around vacancies and dislocations. The strain field in a solid can also be Fourier transformed as in Eq. (2.23) and results in the diffuse scattering (Eq. 2.26). The screened strain field from a point source,

$$u_{\mathrm{p}}(r) = u_0 \frac{\mathrm{e}^{-r/\lambda}}{r^2} \tag{2.31}$$

yields the Fourier transform,

$$u_p(q) = \frac{u_0}{\mathrm{i}q - (1/\lambda)} \approx \frac{u_0}{\mathrm{i}q}, \tag{2.32}$$

resulting in a q^{-2} power law for the intensity when substituted in Eq. (2.26), that is, the diffuse intensity falls off as $1/q^2$ from each Bragg position as with the TDS. Note that the strain field (Eq. 2.31) is not accurate when r is comparable to the atomic distance, at the core of the defect. Indeed it diverges at $r=0$, while such divergence is unphysical. However, the volume of the defect core is small, and its contribution to the Fourier transform is negligibly small.

For general defects, most of the defect can be described as a distribution of point defects, and the strain field due to the defect can be expanded in terms of Eq. (2.31) as

$$u(\mathbf{r}) = \int v(\mathbf{r} - \mathbf{r}') u_{\mathrm{p}}(\mathbf{r}') \mathrm{d}\mathbf{r}'. \tag{2.33}$$

Its Fourier transform is the product of Eq. (2.32) and the form factor, which is the Fourier transform of $v(\boldsymbol{r})$.

$$u(\mathbf{q}) = v(\mathbf{q}) u_{\mathrm{p}}(\mathbf{q}). \tag{2.34}$$

If the defect is localized, the form factor $v(\mathbf{q})$ does not depend too strongly on q, so that the total diffuse scattering follows the q^{-2} law. Thus, the Huang scattering has a similar q dependence as the TDS. They can be differentiated only by studying their temperature dependence, as the Huang scattering is usually independent of temperature. On the other hand, if the defect is spatially extended, the form factor itself may be described by a power law, $v(q) \sim q^{-s}$. Then the total intensity will follow a $q^{-(2+s)}$ power law. In general, the diffuse scattering intensity follows some power law for small q, $q^{-\alpha}$, and the power index α may be related to the effective dimensionality (fractal dimension) of the object (Sinha, 1991).

2.2. CRYSTALLOGRAPHIC ANALYSIS

2.2.1. Rietveld Refinement Method

In the classical method of crystallographic data analysis, each Bragg peak is isolated, a table of the position and integrated intensity for each peak is produced, and the fitting to the calculated position and intensity is attempted. This is still the approach used in single crystal structure determinations, though the process is fully automated by computer. However, this approach severely limits the application of powder diffraction to solving crystal structures because as structures get more complicated, and as Q (or 2θ) increases,

the Bragg peaks get closer together and begin to overlap each other. Structure determination (of unknown structures) from powder diffraction is growing in importance (David *et al.*, 2002), though it is generally not preferred if single crystals are available. After a structure is solved, in the sense that the geometry of the arrangement of the atoms is deduced, by single crystal or powder methods, a process of structure refinement is carried out where atom positions and other structural parameters, such as amplitude of thermal motion, are tweaked using least-squares regression methods in such a way as to get the best possible fit to the measured data. Powder diffraction is very important in refining structural parameters from known structures and indeed is often preferred to single crystal data for this process due to the more kinematical nature of the scattering from a powder. A prior guess at the structural model is made. Then the positions and relative intensities of the Bragg peaks are known. In the Rietveld method (Rietveld, 1969), the whole pattern of diffracted intensity, the diffraction profile, as a function of the diffraction angle 2θ is calculated for the model. This includes modifications to the profile due to experimental effects such as the peak shape, absorption, polarization correction, the DW factor, sample geometry, and the background. The calculated intensity profile, $I_{\mathrm{calc}}(\mathbf{Q})$, is compared to the data, and each parameter of the model is refined to obtain the best-fit structural model. For this purpose, the R-factor (R-factor derives from its name, the residuals function) defined as the difference between the model and experiment,

$$R = \frac{\int \left[I_{\mathrm{meas}}(Q) - I_{\mathrm{calc}}(Q)\right]^2 \mathrm{d}Q}{\int \left[I_{\mathrm{meas}}(Q)\right]^2 \mathrm{d}Q} \tag{2.35}$$

is minimized in a procedure of least square fitting. Ideally R should become zero, but because of various errors it remains nonzero. The residual value of R indicates the quality of the fit. Usually an R-value of a few percent is considered to represent excellent fitting, while a value such as 10% represents rather poor fitting. Other R-factors can also be defined and are used. A common one is the weighted profile R-factor (R_{wp}) in which the statistical significance of each datapoint is taken into account by weighting its contribution to the residuals function. It is defined as

$$R_{\mathrm{wp}} = \frac{\int \left(\frac{1}{\sigma(Q)}\right)^2 \left[I_{\mathrm{meas}}(Q) - I_{\mathrm{calc}}(Q)\right]^2 \mathrm{d}Q}{\int \frac{I_{\mathrm{meas}}(Q)^2}{\sigma(Q)^2} \mathrm{d}Q}, \tag{2.36}$$

where $\sigma(Q)$ is the estimated random error on each datapoint at the level of one standard deviation.

In nearly all current standard Rietveld refinements, the diffuse scattering is dealt with somewhat arbitrarily. If it is widely spread in Q-space, it will be removed with the arbitrary background subtraction. If it is sharply peaked at Bragg peaks (e.g., TDS), it may be included in part as contributing to the Bragg intensity, or it may not be fitted and give rise to a larger R-value. In the high-Q region of the pattern, strongly overlapping Bragg peaks generally mean that even the diffuse scattering that peaked at Bragg peaks may be removed by the background function. Attempts have been made to extract explicit lattice dynamical information from the "background" function by treating it as TDS (Lawson *et al*., 2000). More of these kinds of developments can be expected in the future but are not the subject of this book.

When the Rietveld method was proposed, it met with strong skepticism. However, it is more amenable to modern computers, and with the progress of computer technology it gained popularity. Its power was proven in many instances, including the early days of research on high-temperature superconductors. Whenever a new superconducting compound was discovered, the Rietveld method was used to determine its structure based on structural analogs. Today, it is the standard method of data analysis in powder diffraction. It may be interesting to compare this history with the short history of the use of the PDF method for crystalline materials. It takes a long time for a new method to become developed enough, and widely enough used, to be trusted and accepted. For the method to be widely used, the availability of standard software is crucial. There are a wide variety of Rietveld programs available (e.g., see the programs section of the International Union of Crystallographers (IUCr); Web page: http://www.iucr.org), some of the most commonly used are GSAS (Larson and Von Dreele, 2000), FULLPROF (Rodriguez-Carvajal, 1990), and TOPAS (Coelho, 2004) TOPAS does not just parameterize the diffraction line-shapes but is also one of a variety of programs that implements something called the "fundamental parameters" approach where the line-shapes are calculated taking into account the full physics of the sample and the diffraction experiment. In principle, this results in much better fits to the peaks and allows you to extract more information about things like strain and particle size and size distribution in your sample. Whole powder pattern modeling takes this a step further (Scardi and Leoni, 2002).

2.2.2. Single Crystal Fourier (Patterson) Analysis

In single crystal scattering studies, the Bragg peak intensities are sometimes Fourier transformed. This results in a periodic real-space pair-correlation function known as the crystallographic Patterson function, or just Patterson function (Patterson, 1934). Of more interest to us is to generalize this to the case where the atomic density is continuous, or not periodic.

First, we consider the relationship between the real-space atomic density and the scattering amplitude. Consider the case where the atomic density of

the material under study is not described by a periodic distribution of delta functions but by the continuous density, $\rho(\mathbf{r})$. In this case, Eq. (2.4) becomes

$$\Psi(\mathbf{Q}) = \frac{1}{\rho_0 V}\int \rho(\mathbf{r}) e^{i\mathbf{Q}\cdot\mathbf{r}} d\mathbf{r}, \tag{2.37}$$

where ρ_0 is the average number density of the scatterers. The Fourier back-transform of $\Psi(\mathbf{Q})$ will give $\rho(\mathbf{r})$, the microscopic electron (X-ray or electron scattering) or nuclear (neutron scattering) density; a map of the structure. However, as we have described, we measure only the intensity and not the scattering amplitude directly. The scattering amplitude is proportional to the square root of the intensity, but the phase factor is unknown;

$$\Psi(Q) \propto e^{i\theta}\sqrt{I(Q)}. \tag{2.38}$$

What happens if we Fourier transform the measured intensity instead of $\Psi(\mathbf{Q})$? When properly normalized, the intensity yields the total scattering structure function, $S(\mathbf{Q})$, which is the square of $\Psi(\mathbf{Q})$. Thus,

$$S(\mathbf{Q}) = |\Psi(\mathbf{Q})|^2 = \frac{1}{(\rho_0 V)^2}\int\int \rho(\mathbf{r})\rho(\mathbf{r}')e^{i\mathbf{Q}\cdot(\mathbf{r}-\mathbf{r}')} d\mathbf{r}\, d\mathbf{r}'. \tag{2.39}$$

The Fourier transform of $S(\mathbf{Q})$ is the density–density correlation function called the *generalized Patterson function*. Atomic distances are directly determined by this method, even before determining the whole structure.

As we mentioned above, Patterson maps are often generated in crystallographic studies by Fourier transforming just the Bragg intensities. This results in a discrete sum rather than the continuous integral as shown here. Also, the commonly encountered ones are Fourier difference maps where the difference between the measured and the calculated (from a model) Bragg peak intensities are Fourier transformed to search in real space for inadequacies in the model. The generalized Patterson function described above, where the scattered intensity is a continuous function of $\mathbf{Q}$, is rarely encountered in practice, but is the basis for the PDF as we describe in more detail in Chapter 3.

2.3. CRYSTALLOGRAPHIC METHODS AND DISORDER: LIMITATIONS OF CRYSTALLOGRAPHIC METHODS

While crystallography assumes perfect periodicity, it is possible to include some deviations from periodicity into the analysis. Structural disorder is generally introduced through two parameters:

(a) Enlarged DW factors
(b) Partial occupation of lattice sites

These two crystallographic "band aids" can correctly characterize the extent of local disorder only in limited cases, and they can provide misleading

information on the nature of local disorder. It is worth considering how much disorder in a crystal can be usefully accounted for using these approximations and asking, "What are the limits of crystallographic methods in dealing with disorder?" In this section, we explore some of these limitations and show that the remedial methods for incorporating disorder, such as allowing for enlarged thermal factors, can underestimate and mischaracterize the disorder. This presents a motivation for applying total scattering and PDF methods more widely in the future in situations where it has not traditionally been done. Examples where "solved" structures in the literature were shown to be wrong or incomplete by applying PDF techniques are discussed in Chapters 9 and 10.

2.3.1. DW Factor

Atomic displacements due to phonons are well described by the DW factor that was derived for this purpose (Debye, 1913; Waller, 1923). This method is usually extended to describe other kinds of local disorder than lattice vibrations as well. We will first discuss how to evaluate the DW factor and find whether or not the factor is anomalously large. The DW factor is usually expressed as Eq. (2.18),

$$e^{-Q^2\langle\langle u^2\rangle\rangle} = e^{-2Bs^2}, \qquad B = 8\pi^2\langle\langle u^2\rangle\rangle, \tag{2.40}$$

where $s = \sin\theta/\lambda$. Thus, the DW factor is directly related to the r.m.s. amplitude of lattice vibration, $\langle\langle u^2\rangle\rangle$. Within the Debye model, it can be expressed in terms of the Debye temperature, Θ_D, as,

$$\langle\langle u^2\rangle\rangle = \frac{\hbar}{m\omega}\left(\langle\langle n\rangle\rangle + \frac{1}{2}\right), \qquad \langle\langle n\rangle\rangle = \frac{1}{N}\int_0^{\Theta_D}\frac{\Theta^2 d\Theta}{e^{\Theta/T}-1}, \tag{2.41}$$

where m is the atomic mass. If the phonon density of states, $g(w)$, is known explicitly then $\langle\langle n\rangle\rangle$ can be evaluated explicitly as

$$\langle\langle n\rangle\rangle = \int_0^{\infty}\frac{g(\omega)}{e^{\hbar\omega/kT}-1}d\omega. \tag{2.42}$$

The value of $\langle\langle u^2\rangle\rangle^{1/2}$ is usually less than 0.1 Å at and below room temperature for all the elements. Any DW factor corresponding to a thermal amplitude greater than this is most likely due to the effect of disorder.

It should be noted, however, that extending the DW approximation to describe disorder has serious limitations which are too often not sufficiently recognized. The DW approximation is inaccurate in the following cases:

(i) Strong anharmonicity: If the local potential for an atom is a double-well, the atomic distribution will be bimodal. However, in the DW approximation, this appears simply as a widely distributed atom density in a soft potential (Appendix 2.3).

(ii) Uneven distribution of mean-square displacement amplitudes on crystallographically equivalent sites: If a relatively small number of atoms have larger amplitudes of displacement while others remain normal, fitting one DW factor results in a significant underestimate of the displacements. The atoms with very large displacements are practically ignored.
(iii) Correlated atomic displacements: If two atoms move in the same direction, the change in the interatomic distance is smaller than the displacements of each, and the DW factor overestimates the relative displacements of atoms. On the other hand, if the motions are anticorrelated, the DW factor underestimates the relative displacements.

As an example, let us consider a system in which 60% of the atoms have a root-mean-square displacement amplitude of $u_1 = 0.05$ Å, while the rest of the atoms have an amplitude of $u_2 = 0.2$ Å. The r.m.s. of displacement is then,

$$\langle\langle u^2\rangle\rangle^{1/2} = \left[0.6 \times (0.05)^2 + 0.4 \times (0.2)^2\right]^{1/2} = 0.132. \tag{2.43}$$

Now the total DW factor will be the weighted sum of the two DW envelopes,

$$0.6\exp\left(-\langle\langle u_1^2\rangle\rangle Q^2\right) + 0.4\exp\left(-\langle\langle u_2^2\rangle\rangle Q^2\right). \tag{2.44}$$

If this is approximated by a single DW factor, as shown in Fig. 2.3, the fitted value is

$$\langle\langle u^2\rangle\rangle_{\text{fit}}^{1/2} = 0.062, \tag{2.45}$$

which is barely 1/2 of the true value. If we try to estimate the value of $\langle\langle u_2\rangle\rangle$ by knowing the value of $\langle\langle u_1\rangle\rangle$,

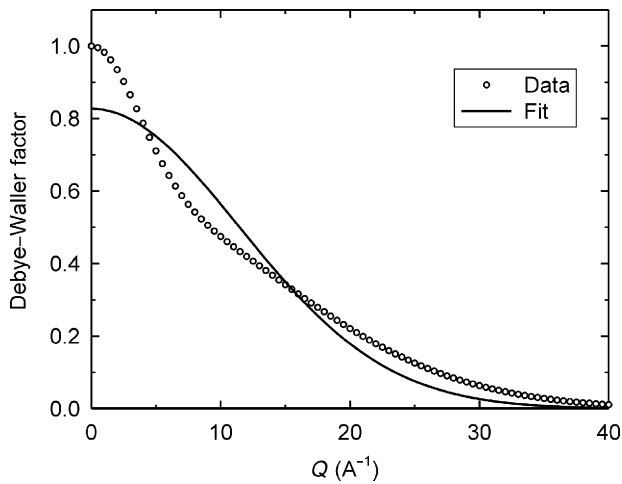

FIGURE 2.3 Debye–Waller factor as a sum of two components (dots) fit with a single component (solid line).

$$\langle\langle u_2^2\rangle\rangle_{\text{fit}} = \left\{\left[\langle\langle u^2\rangle\rangle_{\text{fit}} - 0.6\times(0.05)^2\right]/0.4\right\}^{1/2} = 0.076, \tag{2.46}$$

which is only about 1/3 of the correct value.

This severe underestimate occurred because the DW factor due to $\langle\langle u_2\rangle\rangle$ decreases quickly with Q, as shown in Fig. 2.3, and contributes relatively little to the fitting. For that reason, the DW factor depends upon the range of fitting, as shown in Fig. 2.4. While the case above is a rather extreme case, this example demonstrates the grave danger in estimating the amplitude of displacement for minority atoms by the DW approximation. It is often blindly assumed that even though the DW approximation neglects atomic correlation at least the value of $\langle\langle u^2\rangle\rangle$ determined by the DW factor is correct. This example shows even this assumption should be treated with some caution.

2.3.2. Values of Refined Parameters I: Imperfect Models

As we discussed, because of the crystallographic phase problem structures can only be inferred, and not deduced, from experimental intensity data. This implies that the expected scattering from models must be compared to the observed intensities through a process of "fitting." In any fitting procedure, the results are limited by the accuracy of the underlying model. Inadequacies in the model (e.g., imperfect profile functions, imperfect background subtraction, etc.) have to be accommodated in the fitting process by other degrees of freedom in the model. When this occurs, the refined values of these degrees of

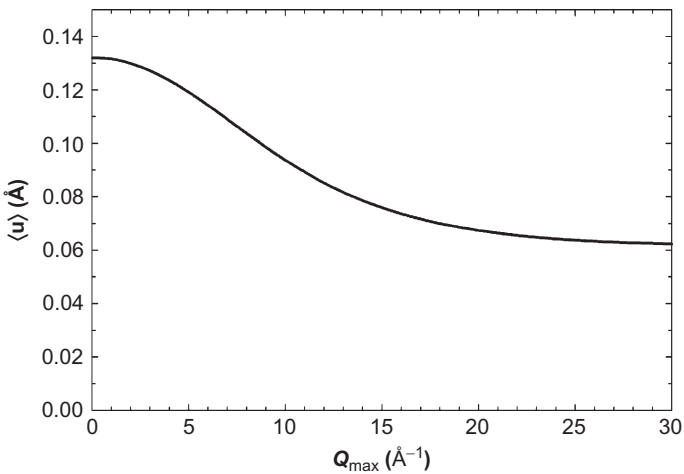

FIGURE 2.4 Value of DW factor as a function of fitting range obtained from fitting a single Gaussian to the two-component Gaussian shown in Fig. 2.3. The "refined" value depends strongly on the range of fitting.

freedom are compromised, or biased in the language of regression. To make this concrete, let us consider an example. Let us assume that the sample has a finite absorption (as all samples do) but that this is not included (or is not correctly incorporated) in the structural refinement. If it is a symmetric flat-plate transmission measurement, the sample absorption increases with increasing diffraction angle as the path length of the rays through the sample increases. Thus, the measured intensity decreases with increasing angle. This appears similar to the effect of the DW factor. The fitting program can (and will) partially correct for this "mistake" by decreasing the overall intensity scale factor and increasing the DW factor somewhat. Because the functional form of the intensity fall off is different from the DW form, the correction is not perfect and there is a concomitant increase in the residuals function. Nonetheless, this illustrates how imperfections in the underlying model bias the refinement leading to unphysical values of certain parameters.

2.3.3. Values of Refined Parameters II: Correlated Parameters

The same example can also be used to illustrate how different parameters in the fit can become correlated. Correlated parameters are also prone to conspire with each other to yield biased, unphysical values. In the example used in the previous paragraph, both the absorption correction and the DW factors give rise to rather slowly varying decreases in the Bragg peak intensities with increasing angle. The difference is in the exact functional form. For instance, for a flat plate in the transmission mode, the absorption correction to the intensity falls off as $\exp(-\mu t/\cos\theta)$, where μt is the absorption length of the sample (measure of how absorbing it is) and $\theta = 2\theta/2$, where 2θ is the diffraction angle. The DW factor falls off as $\exp(-A\sin^2\theta)$, where A is a positive constant (see Eq. 2.41). If we expand the trigonometric terms in the exponents we find that, to leading order, they both yield corrections of the form $A'\exp(-\theta^2)$. They become different only in the terms of higher order. What this means practically is that the Bragg peak intensities need to be fit over a wide range of angle or $\mathbf{Q}$ to reliably differentiate these effects. If the range of fitting is not wide enough, the program does not know whether it should vary the absorption correction or the DW factor, for example. These parameters can then take on arbitrary values provided that, together, they account for the intensity variation adequately. This effect is known as parameter correlation. It can happen to a greater or lesser degree. It is often more dangerous when it happens to a lesser degree because slightly, but not grossly, unphysical parameters will be refined.

The problem of parameter correlation is also exacerbated by the other problem we discussed of an inadequate underlying model. Two partially correlated parameters (such as absorption and the DW factor) may be able to vary in some creative way to account for a fall off in intensity, due to some effect not accounted for in the model, that has a different functional form to

either of them. For example, as discussed in Appendix 2.3, static atomic displacements in the form of a bimodal anharmonic potential whose wells are occupied randomly give rise to an intensity fall off which has a $\cos^2 Q\delta$ functional form, where δ is the magnitude of the displacements. An enthusiastic collaboration between site occupancy factors, scale factor, absorption factor, and DW factor (and possibly other parameters) will be used to accommodate this effect. Exactly how this occurs will also depend on the range over which data are fit. We note that relatively small displacements affect the intensity most strongly at high values of Q. Displacement of atoms by δ will most strongly modify the diffraction intensity around $Q_d = \pi/\delta$. If $\delta = 0.1$ Å, $Q_d = 31$ Å^{-1} which corresponds to a d-spacing of ~ 2 Å, well beyond the range of most crystallographic refinements.

Most modeling programs will report parameter correlations, or at least will list parameters that are correlated by more than a certain amount, say 50%. This program output is widely ignored but is a useful measure of the reliability (or rather unreliability) of certain refined values and should be eagerly checked by the discerning experimentalist. Highly correlated parameters often result in the program diverging and not fitting the data at all. This is easily handled by fixing one of the parameters and not allowing it to vary. The best way to remove error correlations is to introduce into the fit additional information that differentiates the two parameters. Although this is often technologically difficult, it is an increasing trend in the community and has been referred to as "complex modeling" (Billinge and Levin, 2007; Billinge, 2010) in the sense that different experimental and theoretical information sources are being "complexed," or mixed, in the fit.

2.3.4. Values of Rietveld Refined DW Factors: Caveat Emptor

In general, the wider the range over which data are fit, the less acute are the problems of parameter correlations. However, in relation to this, we issue one final caveat emptor. In Rietveld refinement, the range over which data are fitted is usually limited by the problem of Bragg peak overlap at high angles. The acuteness of this problem depends on the symmetry of the material and the resolution of the measurement. Higher symmetry and higher resolution mean that higher values of Q can be fit. For many real-world applications (e.g., high-temperature superconductors measured on standard neutron powder diffractometers), the minimum d-spacing fit is $\sim$0.4–0.5 Å corresponding to a Q_{max} of $\sim$12–15 Å^{-1}. However, with respect to DW factors, higher is not necessarily better. An arbitrary background is subtracted before peak intensities are calculated. This background subtraction is reliable in regions where Bragg peaks do not overlap as the baseline can be seen. An arbitrary functional form is fit to remove residual intensity in these regions. However, in the high-Q region, the Bragg peaks overlap and the baseline is never accessed. The background function is basically extrapolated into this region from its fit

in the low-Q region. In this high-Q region, the Bragg peak intensities are small because of the DW factor. A small error in this extrapolated background could wipe out (or increase) a significant proportion of the real intensity in the Bragg peaks. Also, overlapped Bragg peaks yield craggy peaks sitting on top of a plateau of intensity coming not only from the background and diffuse scattering but also from the overlapping tails of the Bragg peaks themselves. Again, this will result in inaccurate DW factors being refined. Given these problems, it is a miracle that DW factors refined from Rietveld are as good as they are. Caveat emptor: these problems should be borne in mind by the careful reader when assigning significance to Rietveld DW factors.

In the future, for greatest accuracy, it is likely that Rietveld refinements will be carried out on fully corrected $S(Q)$ functions instead of on the raw intensities. In this way, factors such as absorption and backgrounds will not be parameterized in the fit but will be explicitly corrected. This has the disadvantage that significant data processing must be carried out before the fitting is attempted. However, as we describe later, data reduction programs to obtain $S(Q)$ are becoming faster, easier to use, will propagate errors reliably, and maintain data processing histories. All four of these requirements will be necessary to persuade Rietveld aficionados to change from their current approach of fitting raw data. By the same token, more systematic studies are needed of DW factors obtained from PDF fits. Although in principle, they should be more accurate due to the explicit data corrections and the wider range of Q utilized in the fit, in practice, little systematic work has been carried out to verify that the PDF correction and modeling protocols actually do result in more quantitatively accurate DW factors.

APPENDIX 2.1. SCATTERING CROSS-SECTION

Let us consider a beam of particles (photons, neutrons, electrons, etc.) with the wave function,

$$\phi_0 = \mathrm{e}^{\mathbf{ik}\cdot\mathbf{r}}. \tag{A2.1.1}$$

When this wave is scattered by a collection of atoms at $\mathbf{R}_i$, as discussed in Appendix 2.2, the scattered wave is given by ϕ_1 in the first order Born approximation Eq. (A2.2.24),

$$\phi_1 = \frac{\mathrm{e}^{\mathrm{i}kr}}{r}\langle V\rangle \Psi(\mathbf{Q}), \quad \Psi(\mathbf{Q}) = \frac{1}{\langle V\rangle}\sum_i V_i \mathrm{e}^{\mathrm{i}\mathbf{Q}\cdot\mathbf{R}_i}. \tag{A2.1.2}$$

If the flux density of the incoming wave is I_0, the intensity of the scattered beam per area $\mathrm{d}r^2$, $I_\mathrm{s}\,\mathrm{d}r^2$, is given by

$$I_\mathrm{s}\mathrm{d}r^2 = I_\mathrm{s}r^2\mathrm{d}\Omega = I_0|\phi_1|^2 r^2\mathrm{d}\Omega = I_0\mathrm{d}\sigma, \tag{A2.1.3}$$

where σ is the cross-section. Now from Eq. (A2.1.3)

$$\frac{d\sigma}{d\Omega} = |\phi|^2 r^2 = \langle V \rangle^2 |\Psi(\mathbf{Q})|^2. \tag{A2.1.4}$$

APPENDIX 2.2. SAMPLE SCATTERING AMPLITUDE

A2.2.1. Simple Derivation

In the main text of this chapter, we introduced the sample scattering amplitude,

$$\Psi(\mathbf{Q}) = \frac{1}{\langle b \rangle} \sum_v b_v e^{i\mathbf{Q}\cdot\mathbf{R}_v}, \tag{A2.2.1}$$

which forms the basis for the theory of scattering. This equation can be easily deduced as in the following. Let us assume that the incident wave (X-rays, electrons, or neutrons) is described by a wave equation,

$$\phi_{\mathbf{k}_{\text{init}}}(\mathbf{r}) = e^{i\mathbf{k}_{\text{init}}\cdot\mathbf{r}}, \tag{A2.2.2}$$

where $\boldsymbol{k}_{\text{init}}$ is the wavevector (momentum) of the incident wave. In the case of elastic scattering, the scattered wave has the wavevector with the same magnitude but a different direction,

$$\chi_{\mathbf{k}_{\text{final}}}(\mathbf{r}) = A e^{i\mathbf{k}_{\text{final}}\cdot\mathbf{r}}. \tag{A2.2.3}$$

The basis for this expression is the so-called Born approximation, and is given below. However, the phase of this wave may not be same as the incident wave, and that is the point of our interest. When the incident wave reaches the atom v, its amplitude is

$$\phi_{\mathbf{k}_{\text{init}}}(\mathbf{R}_v) = e^{i\mathbf{k}_{\text{init}}\cdot\mathbf{R}_v}, \tag{A2.2.4}$$

where $\mathbf{R}_v$ describes the position of the vth atom. After scattering, the wave changes direction and becomes the scattered wave. The ratio between the amplitudes of the incident wave and the scattered wave is determined by the nature of the scatterer and is independent of the position of the scatterer

$$\chi_{\mathbf{k}_{\text{final}}}(\mathbf{R}_v) = B\phi_{\mathbf{k}_{\text{init}}}(\mathbf{R}_v), \;\; A e^{i\mathbf{k}_{\text{final}}\cdot\mathbf{R}_v} = B e^{i\mathbf{k}_{\text{init}}\cdot\mathbf{R}_v}. \tag{A2.2.5}$$

Therefore

$$A = B e^{i(\mathbf{k}_{\text{init}} - \mathbf{k}_{\text{final}})\cdot\mathbf{R}_v}. \tag{A2.2.6}$$

By expressing B by an absolute value B_0 and the phase, δ,

$$A = B_0 e^{i(\mathbf{k}_{\text{init}} - \mathbf{k}_{\text{final}})\cdot\mathbf{R}_v + i\delta}, \tag{A2.2.7}$$

and the scattered wave is now expressed as

$$\chi_{\mathbf{k}_{\text{final}}}(\mathbf{r}) = B_0 e^{i[(\mathbf{k}_{\text{init}} - \mathbf{k}_{\text{final}})\cdot\mathbf{R}_v + \delta + \mathbf{k}_{\text{final}}\cdot\mathbf{r}]}. \tag{A2.2.8}$$

By defining the scattering vector as

$$\mathbf{Q} = \mathbf{k}_{\text{init}} - \mathbf{k}_{\text{final}} \tag{A2.2.9}$$

we obtain

$$\chi_{\mathbf{k}_{\text{final}}}(\mathbf{r}) = F(\mathbf{Q})\chi_0(\mathbf{r}),\ \ F(\mathbf{Q}) = \mathrm{e}^{\mathrm{i}\mathbf{Q}\cdot\mathbf{R}_v},\ \ \chi_0(\mathbf{r}) = B_0\mathrm{e}^{\mathrm{i}\delta}\mathrm{e}^{\mathrm{i}\mathbf{k}_{\text{final}}\cdot\mathbf{r}}. \tag{A2.2.10}$$

Finally, superposing the amplitudes of the waves scattered from each atom by summing over v, we obtain the static structure factor for the total wave scattered by an assembly of N scattering objects (atoms),

$$\chi_{\mathbf{k}_{\text{final}}}(\mathbf{r}) = F(\mathbf{Q})\chi_0(\mathbf{r}),\ \ F(\mathbf{Q}) = \frac{1}{\langle b\rangle}\sum_v b_v\mathrm{e}^{\mathrm{i}\mathbf{Q}\cdot\mathbf{R}_v}. \tag{A2.2.11}$$

A2.2.2. Born Approximation

A more rigorous derivation is the standard Born approximation (e.g., Wu and Ohmura, 1962). The total wavefunction, ϕ, is the sum of the incoming and outgoing waves and satisfies the Schrödinger equation,

$$\left(-\frac{\hbar^2}{2m}\nabla^2 + \lambda V\right)\phi = E\phi, \tag{A2.2.12}$$

where $V(\boldsymbol{r})$ is the scattering potential located near the origin, and λ is a controlling variable which will be equated to unity after the analysis. At large values of $\boldsymbol{r}$, $V = 0$, so that

$$E = \frac{\hbar^2\mathbf{k}_{\text{init}}^2}{2m},\ \ \phi_{\text{init}}(\mathbf{r}) = \mathrm{e}^{\mathrm{i}\mathbf{k}_{\text{init}}\cdot\mathbf{r}}. \tag{A2.2.13}$$

We now consider expanding ϕ by λ:

$$\phi = \phi_0 + \lambda\phi_1 + \lambda^2\phi_2 + \cdots. \tag{A2.2.14}$$

Then Eq. (A2.2.12) becomes, equating each order in λ,

$$\begin{aligned}
-\frac{\hbar^2}{2m}\nabla^2\phi_0 &= E\phi_0,\\
\left(-\frac{\hbar^2}{2m}\nabla^2 - E\right)\phi_1 &= -V\phi_0,\\
\left(-\frac{\hbar^2}{2m}\nabla^2 - E\right)\phi_2 &= -V\phi_1,\\
&\vdots
\end{aligned} \tag{A2.2.15}$$

Thus,

$$\phi_0 = \phi_{\text{init}}. \tag{A2.2.16}$$

To solve for the first order scattered wave ϕ_1, we have to consider the Greens function,

$$\left(-\frac{\hbar^2}{2m}\nabla^2 - E\right)G(\mathbf{r}-\mathbf{r}') = \delta(\mathbf{r}-\mathbf{r}'), \tag{A2.2.17}$$

$$G(\mathbf{r}-\mathbf{r}') = \frac{e^{ik|\mathbf{r}-\mathbf{r}'|}}{4\pi|\mathbf{r}-\mathbf{r}'|}. \tag{A2.2.18}$$

Thus,

$$\phi_1 = \frac{1}{4\pi}\int \frac{e^{ik|\mathbf{r}-\mathbf{r}'|}}{|\mathbf{r}-\mathbf{r}'|}V(\mathbf{r}')e^{i\mathbf{k}\cdot\mathbf{r}'}d\mathbf{r}'. \tag{A2.2.19}$$

At large distance ($r \gg r'$),

$$|\mathbf{r}-\mathbf{r}'| \approx r - r'\cos\theta, \tag{A2.2.20}$$

where θ is the angle between $\mathbf{r}$ and $\mathbf{r}'$. Then,

$$k|\mathbf{r}-\mathbf{r}'| \approx kr - \mathbf{k}'\cdot\mathbf{r}', \tag{A2.2.21}$$

where $\mathbf{k}'$ is a wavevector parallel to $\mathbf{r}$ and $|\mathbf{k}'|=$k. Thus Eq. (A2.2.19) becomes

$$\phi_1 \approx \frac{e^{ikr}}{4\pi r}\int V(\mathbf{r}')e^{i(\mathbf{k}-\mathbf{k}')\cdot\mathbf{r}'}d\mathbf{r}'. \tag{A2.2.22}$$

Here the multiplier represents a spherical wave. If the scattering potential is a collection of nuclear potentials at the atoms in the solid,

$$V(\mathbf{r}) = \sum_i V_i\delta(\mathbf{r}-\mathbf{R}_i). \tag{A2.2.23}$$

Then the scattered wave is given by

$$\phi_1 = \frac{e^{ikr}}{r}\langle V\rangle\Psi(\mathbf{Q}), \quad \Psi(\mathbf{Q}) = \frac{1}{\langle V\rangle}\sum_i V_i e^{i\mathbf{Q}\cdot\mathbf{R}_i}, \tag{A2.2.24}$$

which leads to Eq. (A2.2.1).

APPENDIX 2.3. DIFFRACTION SIGNATURE OF ATOMIC DISPLACEMENTS

To illustrate how the signature of a non-Gaussian distribution of atomic displacements shows up in the diffraction pattern, let us consider a one-dimensional chain of atoms separated by a, displaced by δx, in alternating directions on neighboring sites. This happens if the local potential of an atom is double-well, and there is an antiferroelectric correlation among the displacements. The atomic position is then given by,

$$R_v = va + \delta x e^{iv\pi}. \tag{A2.3.1}$$

Then the crystallographic structure factor is,

$$\begin{aligned} F(Q) &= \sum_v e^{iQR_v} = \sum_\mu \left[e^{iQ\delta x} + e^{iQ(a-\delta x)}\right] e^{i2Q\mu a}, \\ &= 2N \sum_n \left[\delta\left(Q - \frac{2n\pi}{a}\right)\cos(Q\delta x) + i\delta\left(Q - \frac{(2n+1)\pi}{a}\right)\sin(Q\delta x)\right]. \end{aligned} \tag{A2.3.2}$$

Thus, if δx is small, the superlattice diffraction peaks at $Q = (2n+1)\pi/a$ have the intensity proportional to $\sin^2(Q\delta x)$, with the maximum intensity appearing at $Q = \pi/(2dx)$. If δx is ~ 0.1 Å, this corresponds to a $\mathbf{Q}$ of 15.7 $Å^{-1}$. This is why the signature of displacements appears at high values of Q. At low Q, the intensity is proportional to $\delta x^2 Q^2$. This Q^2 dependence is recovered in the derivation for the diffuse scattering. The main Bragg peaks at $Q = 2n\pi/a$ are modulated by $\cos^2(Q\delta x)$. At small values of Q, this is approximately

$$\cos^2(\mathbf{Q}\delta x) = 1 - \frac{1}{2}(Q\delta x)^2 + \cdots \approx e^{-Q^2\delta x^2/2}. \tag{A2.3.3}$$

Thus, the effect of these displacements merely adds to the DW factor. If the directions of displacements are not ordered but random, Eq. (A2.3.2), is

$$\begin{aligned} F(Q) &= \sum_v e^{iQR_v} = \sum_v e^{i\,\mathrm{sign}(v)Q\delta x} e^{i2Qva}, \\ &= 2N \sum_v [\cos(Q\delta x) + i\,\mathrm{sign}(v)\sin(Q\delta x)] e^{i2Qva}, \\ &= 2N\cos(Q\delta x) \sum_n \delta\left(Q - \frac{2n\pi}{a}\right), \end{aligned} \tag{A2.3.4}$$

where sign(v) is randomly $+1$ or -1. Thus the superlattice peaks would not be present but the intensity of the fundamental Bragg peaks is modulated by $\cos^2(Q\delta x)$. Thus, as in Eq. (A2.3.3), it is not easy to differentiate this factor from the DW factor unless Q is larger than $\pi/\delta x$. This is why the DW approximation has undeserved successes, as crystallographic analysis is usually done in the low-Q region below $\pi/\delta x$.

REFERENCES

Abeykoon, M., Malliakas, C.D., Juhás, P., Bozin, E.S., Kanatzidis, M.G. & Billinge, S.J.L. (2012) *Z. Kristallogr.*, **227**, 248.

Bacon, G.E. (1975) *Neutron Diffraction*. Oxford: Clarendon Press.

Billinge, S.J.L. & Levin, I. (2007) *Science*, **316**, 561.

Billinge, S.J.L. (2010) *Physics*, **3**, 25.

Borie, B. (1957) *Acta Crystallogr.*, **10**, 89.

Borie, B. (1959) *Acta Crystallogr.*, **12**, 280.
Borie, B. (1961) *Acta Crystallogr.*, **14**, 472.
Cockayne, D.J.H. (2007) *Annu. Rev. Mater. Res.*, **37**, 159.
Coelho, A.A., 2004. TOPAS: general profile and structure analysis software for powder diffraction data. http://www.topas-academic.net/.
David, W.I.F., Shankland, K., McCusker, L.B. & Baerlocher, Ch. (2002) *Structure Determination from Powder Diffraction Data*. Oxford: Oxford University Press.
Debye, P. (1913) *Verh. D. Deutsch. Phys. Ges.*, **15**, 678 738, 857.
Giacovazzo, C., Monaco, H.L., Viterbo, D., Scordari, F., Gilli, G., Zanotti, G. & Catti, M. (1992) *Fundamentals of Crystallography International Union of Crystallography Monograph*. Oxford: Oxford Science Publications.
Huang, K. (1947) *Proc. R. Soc. A*, **190**, 102.
Jeong, I.K., Mohiuddin-Jacobs, F., Petkov, V., Billinge, S.J.L. & Kycia, S. (2001) *Phys. Rev. B*, **63**, 205202.
Larson, A.C., Von Dreele, R.B., 2000. General Structure Analysis System (GSAS), Los Alamos National Laboratory Report LAUR, 86.
Lawson, A.C., Martinez, B., Von Dreele, R.B., Roberts, J.A., Sheldon, R.I., Brun, T.O. & Richardson, J.W. (2000) *Phil. Mag. B*, **80**, 1869.
Miao, J., Charalambous, P., Kirz, J. & Sayre, D. (1999) *Nature*, **400**, 342.
Moss, S.C. & Graczyk, J.F. (1969) *Phys. Rev. Lett.*, **23**, 1167.
Patterson, A.L. (1934) *Phys. Rev.*, **46**, 372.
Rietveld, H.M. (1969) *J. Appl. Crystallogr.*, **2**, 65.
Rodriguez-Carvajal, J., 1990. FULLPROF: A Program for Rietveld Refinement and Pattern Matching Analysis, Abstracts of the Satellite Meeting on Powder Diffraction of the XV Congress of the IUCr, Toulouse.
Sayre, D. (1952) *Acta Crystallogr.*, **5**, 843.
Scardi, P. & Leoni, M. (2002) *Acta Crystallogr.*, **A58**, 190.
Sinha, S.K. (1991) *Phys. B*, **173**, 25.
Waller, I. (1923) *Zeit F. Phys.*, **17**, 398.
Warren, B.E. (1990) *X-ray Diffraction*. New York: Dover.
Woolfson, M.M. (1997) *An Introduction to X-ray Crystallography* (2nd Edition). Cambridge: Cambridge University Press.
Wu, T.Y. & Ohmura, T. (1962) *Quantum Theory of Scattering*. Englewood Cliffs: Prentice-Hall.
Zuo, J.M., Vartanyants, I., Gao, M., Zhang, R. & Nagahara, L.A. (2003) *Science*, **300**, 1419.

General Texts on Electron Diffraction

Cowley, J.M. (1995) *Diffraction Physics* (3rd Edition). Amsterdam: North-Holland Personal Library, Elsevier.
Fultz, B. & Howe, J.M. (2009) *Transmission Electron Microscopy and Diffractometry of Materials* (3rd Edition). Berlin: Springer.
Williams, D.B. & Carter, C.B. (1996) *Transmission Electron Microscopy: A Textbook for Materials Science, Vols. 1–4*. New York: Plenum.

Diffuse Scattering

Billinge, S.J.L., & Thorpe, M.F. (Eds.), (1998). *Local Structure from Diffraction*. New York: Plenum Press.
Krivoglaz, M.A. (1969) *Theory of X-Ray and Thermal-Neutron Scattering by Real Crystals*. New York: Plenum Press.

Krivoglaz, M.A. (1996) *Diffuse Scattering of X-Rays and Neutrons by Fluctuations.* Berlin: Springer.

Nield, V.M. & Keen, D.A. (2001) *Diffuse Neutron Scattering from Crystalline Materials. Oxford Series on Neutron Scattering in Condensed Matter* Oxford: Clarendon Press.

Schweika, W. (1998) *Disordered Alloys: Diffuse Scattering and Monte Carlo Simulations, Tracts in Modern Physics.* Berlin: Springer.

Welberry, T.R. (2004) *Diffuse X-ray Scattering and Models of Disorder.* Oxford: Oxford University Press.

Lattice Vibrations

Born, M. & Huang, K. (1954) *Dynamical Theory of Crystal Lattices.* Oxford: Oxford University Press.

Willis, B.T.M. & Pryor, A.W. (1975) *Thermal Vibrations in Crystallography.* Cambridge: Cambridge University Press.